Safe Close-Proximity and Physical Human-Robot Interaction Using Industrial Robots

Danial Nakhaeinia, Pascal Laferrière, Pierre Payeur, Robert Laganière
Sensing and Machine Vision for Automation and Robotic Intelligence Research Group
University of Ottawa
Ottawa, ON, Canada
[dnakhaei, plafi092, ppayeur, laganier]@uottawa.ca

***Abstract*—Industrial robots have been employed worldwide in the manufacturing sector for performing tasks quickly, repeatedly and accurately in relatively static environments for over 30 years. In recent years, close physical interaction between industrial robots and human operators has attracted researchers' attention and encouraged a number of technological innovations to turn these robots into human-robot platforms. In this work a specially designed compliant wrist is developed to support dexterous robotic interaction with live proximity and contact feedback. The compliant wrist incorporates a level of compliance into an initially non-compliant manipulator robot which allows the robot to dynamically adapt to the surfaces it approaches or touches. Furthermore, to facilitate human–robot interactions, the robot must be able to adapt its behavior to the human partner. Therefore, a real-time path planning method is developed to generate online motion, adapt the robot to dynamic changes in the environment and ensure smooth interactions. The performance of the proposed method is demonstrated through experimental results on a CRS-F3 manipulator.**

Keywords-human-robot interaction; compliant wrist; industrial robots; real time system; motion planning; robotics; proximity and contact feedback;

I. INTRODUCTION

Industrial robots rapidly gained popularity in manufacturing because of their quick, continuous and accurate operation in inhospitable or hazardous environments for humans. However, in modern manufacturing, robots have frequently changing applications and being repurposed for alternate tasks. In order to accomplish this, more intricate user interfaces and special means for interacting with the new surroundings are often developed to meet the different requirements. This is especially true when a human element is introduced into the workspace. Enabling humans and robots to work together is a challenging issue and applications requiring this of robots highlight certain difficulties that are faced. For example, industrial robots, which are generally designed and programmed to work in static environments tend to have poor adaptability to dynamic environments preventing them from easily being re-tasked [1]. According to [2], in some cases making a robot such as those found in industrial applications behave gently and safely is an almost hopeless task due in particular to their large masses and rigid constructions. In order to extend the usability of industrial robots from factories to human environments the issues of safety and flexibility must be resolved, a task that has yet to be fully achieved even in the industrial scenarios. Therefore, innovative technologies should be developed to allow these robotic platforms to interact and communicate with humans while still maintaining a satisfactory level of safety for operators, or bystanders, as the case may be. Inspired from the human-like adaptable compliance, robots should have similar capabilities embedded in biological systems in order to safely interact with humans. The major problem with the existing industrial robots is the absence of compliance or variable stiffness [3]. Attempts have been made at constructing intrinsically safe robots by incorporating compliant structures directly into the actuators [4][5].

Human-robot interaction can be classified into three distinct categories: remote interaction, proximity interaction and physical interaction. Each category is differentiated by the distance between the human and the robot [6]. In remote interaction, the human and the robot work in separate environment and there is no direct interaction between them. The user controls the robot motion remotely using an interface. The remote interaction approaches [7][8] have been mainly proposed to direct the robots from a distance with the purpose of supporting and cooperating with humans in order to accomplish a specific task. In proximity interaction, the robot and the user work in close proximity to each other and they share the same space but typically there is no direct contact between the two [9]. Lasota et al. [10] proposed a real-time safety system for human-robot interaction at very low distances with industrial robots. This approach does not require hardware modifications or part replacements and instead utilizes the robot joint angles and accurate human localization via the construction of a real-time virtual representation of the workspace. The authors later presented an adaptive motion-planning technique [11] to avoid potential motion conflicts in close-proximity human–robot interaction which uses the prediction of human actions and a workspace occupancy model. Mainprice and Berenson [12] developed a collaborative manipulation framework for simultaneous human-robot motion in close proximity based on early prediction of the human motion. In this framework the probabilistic models learned in the offline phase are used to detect the human's intent and predict the workspace occupancy for planning trajectories with minimal penetration costs for the workspace. However, in physical interaction, the human has direct physical contact with the robot. They are co-located and work together as companions or human-robot teams in the same room. In [13], a motor

978-1-4799-1986-4/15 $31.00 © 2015 IEEE
DOI 10.1109/CRV.2015.38

learning system was developed for physical human-robot interaction (PHRI) wherein the proposed control system takes advantage of inherent joint flexibility and relies on physical help from a human. A machine learning algorithm was also presented in [14] for PHRI, based on a dimensional reduction technique allowing a robot to adapt its behavior. It creates a behavioral model according to the actions of the human counterpart. Norouzzadeh et al. [15] proposed an online optimal control method which imposes constraints on interaction forces, position, and velocity of the robot to ensure safe physical human-robot interaction.

While a significant amount of experimentation aimed at integrating industrial robots in collaborative human-robot applications has been conducted, the majority has required hardware modifications, retrofitting and new components that can be prohibitively costly or even physically impossible to achieve. The goal of this work is to address the flexibility and safety issues of industrial robots for physical and proximity interactions with humans without the need for retrofitting the robotic platform or making significant hardware modifications such as including new actuators or adding internal joint sensors. We attempt to solve the flexibility problem through the use of an adaptable compliant wrist [15] designed to incorporate a degree of compliance onto an initially non-compliant manipulator providing a greater degree of flexibility and adaptability for physical and proximity human-robot interaction.

To ensure physical safety and prevent any damage, injury and unwanted contact in a shared work space, a reliable path planning algorithm is required to direct the robot motion under consideration of the human partner. This work introduces a real-time path planning method and a possible application for the compliant wrist, namely online motion generation using live proximity and contact feedback, providing the ability to adapt the robot to the dynamic changes and uncertainties in close proximity and contact with humans or objects in the environment.

The following section gives an overview of the previously developed instrumented compliant wrist which provides the primary feedback information used in the path planning control loops. Sections III and IV present the proposed proximity and physical interaction motion planning control strategies, respectively. Several experiments were conducted to validate the control strategies and determine the viability of the compliant wrist as an effective source of motion and contact feedback. The results of those experiments are presented in section V and discussed further in Section VI. Conclusions derived from our experimentation are presented in Section VII.

II. INSTRUMENTED COMPLIANT WRIST

As previously discussed, compliance is an essential feature for robotic platforms in human-robot applications. Compliance allows for greater margins of uncertainty in sensing technologies meant to describe the motion and position of the objects surrounding a robot by reducing the risk of damages in situations where such measurement errors could be hazardous. The compliant wrist mentioned previously can easily be attached to the end effector of a manipulator robot providing it with a means of detecting objects both in contact and proximity to the end effector, as well as adding a degree of compliance to the end effector. The physical structure of the wrist is made up of a movable planar contact surface which allows the wrist to sense angular and translation disturbances. It achieves its compliance and motion via an antagonistic spring system. The system is composed of a larger central compression spring and four smaller elastic components located in the corners of the structure. These all act together to produce continuous tension on the device and allow it to maintain a rest state when no external forces are applied. The original conception of the compliant wrist is shown in Fig. 1. Since the publication of [15], it has undergone a few minor changes in order to address some key issues, namely an increase in the amount of translational compliance available by lengthening the central shaft, as well as an outward extension of the external sensor mounting brackets meant to negate the effects of interference caused by the first modification. By increasing the distance of the movable plate, it entered into the field of view of the sensors which produce a cone shaped beam of infrared light rather than a narrow beam. Also, the external springs were replaced with elastic cord due to its ease of length modification as compared to metal springs. Fig. 2 shows the fully assembled device including an electronics enclosure which forms the base of the device.

The compliant wrist is equipped with a battery powered microcontroller, a wireless communications interface and eight infrared distance measurement sensors to form a self-contained module. The microcontroller is responsible for recording the distance measurements from the sensors, providing digital signal processing capabilities such as filtering, making the necessary calculations to extract meaningful data from the distance measurements and transmitting the information to external sources upon receiving requests from them. The infrared sensors are arranged in two arrays of four sensors each, with the one array being referred to as the external array and the other as

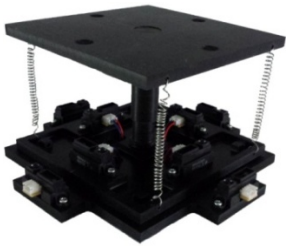

Fig. 1. Compliant wrist original prototype.

Fig. 2. Updated version of the compliant wrist prototype.

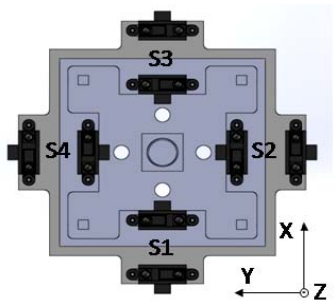

Fig. 3. Sensor arrangment.

the internal array.

The external sensor array is situated on the compliant wrist in such a way that allows it to measure distances at multiple points between the wrist and object surfaces located in front of the end effector. The internal sensor array is situated between the base of the compliant wrist structure and the moveable plate providing the structure's compliance. Both of these sensor arrays allow the device to determine rotations about two axes, X and Y, and a translation distance. From these parameters it is possible to provide object pose estimations in the form of a 3D homogeneous transformation matrix. The external sensor array provides the proximity detection functionality while the internal sensor array provides contact feedback information. Both sensor arrays are mounted onto the compliant wrist in a specific pattern thereby facilitating the definition of a coordinate system to be used as a reference frame assigned to the wrist. The sensors in each array are numbered from 1 to 4 with the reference frame axes defined as shown in Fig. 3.

The extraction process of the rotation and translation parameters relies solely on distance measurements obtained from the IR sensors. Each rotation angle is calculated from the distance measurements of two IR sensors aligned along a particular axis. The rotation about the X axis is extracted from the distances measured by the two sensors aligned along the Y axis, and the rotation about the Y axis is extracted from the distances measured by the two sensors aligned along the X axis. By taking the arctangent of a right angle triangle whose vertical side is the difference in distance measurements of the two sensors on that axis with a base whose length is equal to the distance that separates the two sensors, the desired angle is obtained. An example of how the rotation angle about the Y axis is calculated, using the distances measured from two sensors aligned along the X axis, is given on the right of Fig. 4, assuming an in-between sensor distance of *W*. Rotations can be calculated according to Eq. (1) and (2) where *S* indicates a sensor distance, the subscripted letters denote the axis of alignment and the positive or negative signs denote on which side of the center of the axis these sensors are positioned.

$$R_X = atan2(S_{Y+} - S_{Y-}, W) \quad (1)$$

$$R_Y = atan2(S_{X-} - S_{X+}, W) \quad (2)$$

The translation along the Z axis is also obtained from the distance measurements of two sensors aligned along a particular axis. By taking the average of both distance measurements we can find the distance between the centers of the upper and lower plates. This is possible due to the symmetry of the sensor placement. Eq. (3) defines how the translation is calculated using the distances measured from two opposite sensors. An example is given on the left side of Fig. 4. Either pair of sensors along an axis can provide an estimate of the translation; however, the value will only be the same for both pairs if the surface is planar as seen by all four sensors in the set.

$$T_z = \frac{S_{X-}+S_{X+}}{2} = \frac{S_{Y-}+S_{Y+}}{2} \quad (3)$$

An example of how the transformation matrix is calculated from the internal sensor distances is given in Eq. (4). Fig. 5 provides a reference for the values used in the matrix calculation. A, B, C, D are the distance values measured by internal sensors 1, 2, 3 and 4, respectively. A similar calculation can be made from the external sensors using values E, F, G and H which are measured by external sensors 1, 2, 3 and 4 respectively.

The equivalent homogeneous transformation, $Q_{compliant/effector}$, between the two plates is defined as follows:

$$Q_{compliant/effector} = \begin{bmatrix} \cos\alpha & 0 & \sin\alpha & 0 \\ \sin\beta\sin\alpha & \cos\beta & -\sin\beta\cos\alpha & 0 \\ -\cos\beta\sin\alpha & \sin\beta & \cos\beta\cos\alpha & \frac{A+B+C+D}{4} \\ 0 & 0 & 0 & 1 \end{bmatrix} \quad (4)$$

where $\beta = atan2(^{D-B}/_{W})$ and $\alpha = atan2(^{A-C}/_{W})$.

III. Proximity Interaction

Close proximity interaction is still a fairly new topic andis still undergoing much development. While there is not a specific definition of safety in this context, in order to prevent collision with objects or humans, fast and accurate online motion planning is typically required when humans

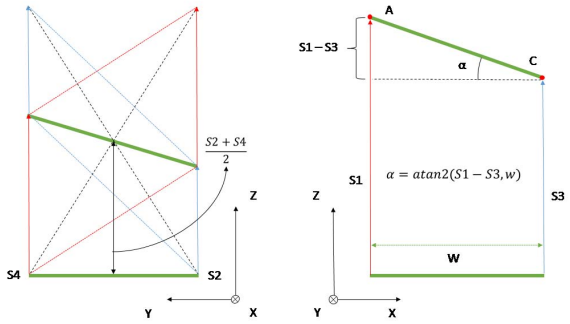

Fig. 4. Extracted distance measurements from internal and external sensors.

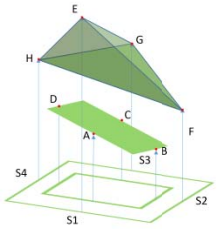

Fig. 5. Distance measurements from internal and external sensors.

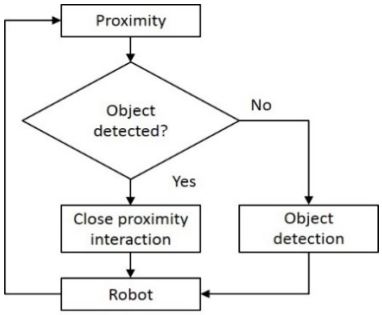

Fig. 6. Proximity interaction flowchart.

and robots are working together in close proximity. This work proposes a real-time adaptation method in which the robot imitates the motion of a human partner and follows it into a specific pose. The robot follows the selected target's motion direction while maintaining a safe distance from it and also attempts to match its orientation. In order to maintain this safe distance a fuzzy controller is employed to steer the robot. The robot either moves toward or away from the target as the target moves away from or toward the robot, respectively. Fig. 6shows the proposed proximity interaction method flowchart diagram.

A. Object Detection

Due to the physical characteristics of the compliant wrist, specifically the distance between each of the sensors that make up the external array, pose estimation returns the most accurate orientation results when all four sensors in the array are able to detect a target. Therefore, whenever an object isnot being detected by all of the sensors in the external array, an object search algorithm is invoked. This algorithm is meant to guide the robot in the direction that has the highest likelihood of allowing all of the sensors to return avalid distance measurement indicative of an object present in front of the end effector. The infrared sensors have a maximum range of detection which is approximately 400mm and continuously return this value even when no object is present in front of the sensors. Therefore, in order to differentiate between the situation of having no object present and when an object is present, a lesser distance value must be measuredtodiscriminate between the two cases. This lesser measurements are deemed valid. Based on the available sensory information, the robot moves by a specified increment in position in one of eight different directions. The directions are defined with respect to the end effector's reference frame and can be either -X, -Y, +X, +Y or certain combinations of these. As shown in Table 1, a set of If-Then rules are considered to decide in which direction to steer the robot. For exampleif only the sensors S_1 and S_2 detect an object, the robot moves in the –X and -Y direction with respect to the wrist frame. In order to achieve this motion, since the robot can be in any pose when the object is detected, the target position is transformed to the robot base frame as shown in Eq.(5).

$$^{B}P_T = Q_{base/wrist} \cdot {}^{w}P_T \quad (5)$$

Table 1. Object searching rules.

If	*Then*	Direction	If	*Then*	Direction
None		N/A	S3 , S4		+X & +Y
S1		-X	S4 , S1		+Y & -X
S2		-Y	S1, S2, S3		-Y
S3		+X	S2, S3, S4		+X
S4		+Y	S3, S4, S1		+Y
S1, S2		-X & -Y	S4, S1, S2		-X
S2 , S3		-Y & +X	S1, S2, S3, S4		N/A

$^{W}P_T$ represents the target point with respect to the wrist frame, Q_{BW} is the homogenous transformation between the wrist and the robot base and $^{B}P_T$ is the target position with respect to the base frame. The target point information is extracted from the transformation matrix obtained directly from the compliant wrist's sensors.

B. Close Proximity Interaction

If the object search algorithm is able to successfully locate an object with the external sensor array, the close proximity interaction module is activated and the robot tracks and follows the target object's motion direction and orientation while maintaining a safe distance away from the object. To significantly reduce the number of design parameters, a simplified SISO fuzzy controller is designed to control the desired separation distance during the interaction smoothly. The proposed fuzzy controller input (D_z) is the average distance of the external sensors and the output (M_d) is the direction of movement of the robot. Given that there are four sensors in the external sensory layer, four points in three dimensions are obtained. The distance from the object (D_z) is calculated by taking the average of the distances measured by the external sensors as in Eq. (6).

$$D_z = \sum_{i=1}^{4} S_i/4 \quad (6)$$

The input's membership functions are: close, safe and far. These functions and their values are shown in the upper half of Fig. 7. The output's membership functions are backward (or away from object), constant and forward (toward theobject), shown in the lower half of Fig. 7. A

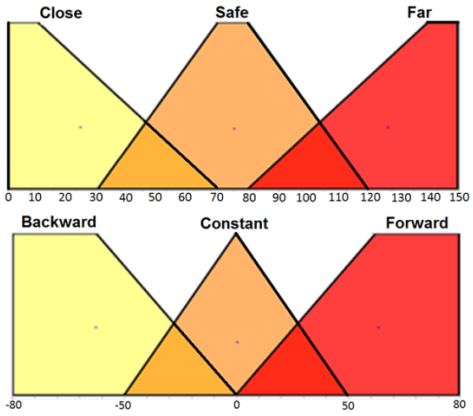

Fig. 7. Fuzzy set definitions for input variable (average sensor distance in mm) (top) and output variable (motion direction in mm) (bottom).

simplified linear fuzzy rule base is defined to convert the fuzzy input sets to outputs as

Rule #i: IF D_z is *Close* THEN M_d *is Backward*

The centroid defuzzifier, Eq. (7), is used to calculate the output.

$$M_d = \frac{\sum_{i=1}^{N} \mu_i.(a_i.D_z+b_i)}{\sum_{i}^{N} \mu_i} \quad (7)$$

Where $\mu_i$is the output membership for the rule *#i,a* and *b* are the design parameters that are determined by the user. The fuzzy output changes based on the target's distance from the robot to prevent any unwanted contact between the robot and a person. In addition to tuning the separation distance the robot attempts to match the object's orientation. As explained in section II, the orientation is also calculated using the distances measured by the external sensors. Since the orientation is with respect to the wrist frame, it is also transformed to the robot base frame in a similar fashion as described in Eq. (5).

IV. Physical Interaction

For successful physical human-robot interaction (PHRI) the robot is required to be able to adapt its behavior to the human partner who can behave in an unpredicted way. This task usually includes three motion modes: free motion, transition and compliant motion. Free motion refers to the robot movement in an unconstrained work space, the transition mode falls somewhere between the free motion and the compliant motion modes and is meant to ensure a safe approach, and the compliant mode is activated when there is direct physical contact between the robot and human [3]. Each of the specific motion modes requires a different set of design considerations during their implementation. The compliant layer of the designed compliant wrist allows the robot to adapt to the changes and forces generated by the surfaces with which it comes into contact. It should be noted that the actual forces being applied to the compliant wrist are not measured in any way. This is akin to humans who can feel forces being applied to the body, lacking means of precisely measuring those forces, but are nevertheless able to react to them when sensed. Furthermore, it enables someone to physically guide the robot to a specific pose by providing the sensors with the necessary information to move as desired. In order to dynamically react to the forces and adapt the robot to the human behavior a precise motion control strategy is required. Fig. 8shows the proposed control system flowchart which involves the three modes of motion required for PHRI tasks. This can be done in either of the modes of motion we have considered in our algorithm. The two modes are distinguished by the distance values return by all of the sensors, both internal and external. Firstly, the distance values of the internal sensors are verified in order to determine if we are in contact with an object. If no object is found to be in contact with the contact plate, the external sensors distances are examined to determine if an object is within the field of view. In both cases, if any of the distance values meet the requirements for that particular case, an attempt is made at moving the robot into the estimated pose. When dealing with the external sensors, we are operating in the transition mode. As for when contact is detected, we are said to be operating in the constrained mode.

As explained in section III, the first step is object detection in which the robot is adjusted to maximize the accuracy of pose estimations prior to attempting to approach the detected object. Once the object is sufficiently detected the transition mode is activated. The proximity (external) sensors provide the local information about the object's position and orientation with respect to the robot's end effector. The pose calculated using the proximity sensors is set as the target point with which we wish to align the end effector. This is done with the objective that by matching the orientation of the object's surface, the risk of injury or damage will be minimized prior to making contact. When contact is detected by the internal sensors, the compliant motion mode is activated. Contact is detected much in the way that object detection is performed and requires a threshold distance in order to distinguish true contact from the rest state of the compliant wrist's contact plate which provides the compliant interface between the wrist and objects. The compliance is obtained from the fact that this contact plate can be deflected under externally applied forces. The instrumentation of the compliant wrist is capable of continuously measuring this deflection which provides additional information about the object and the contact point. This enables the robot to more precisely adapt and compensate for errors due to dynamic changes. Such changes often occur in real world scenarios such as when a person is touched. When this happens, it is quite normal for that person to react to the new stimulus and they will very rarely maintain a constant position.

V. Experimental Setup

In order to begin characterization of the performance of the compliant wrist three experimental protocols were devised and carried out with a 7-DOF CRS F3 manipulator robot to which the compliant wrist was attached to act as its end effector tool. During the experiments sensor data was

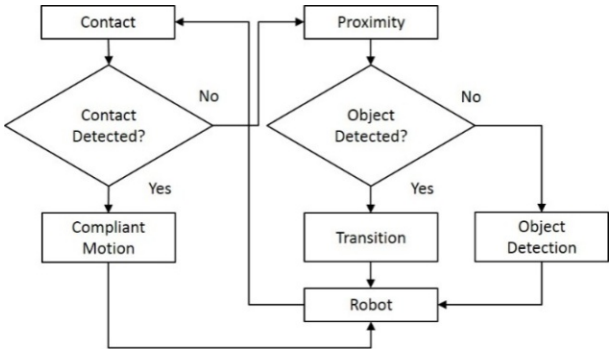

Fig. 8. Control system flowchart.

transmitted to the control system via a wireless radio connection and power was provided by an AC adapter for convenience. In all cases sensor data were acquired at a rate of 50 Hz and a moving average filter with a window length of 33 was applied to the raw samples of each IR sensor as a preprocessing step. Also, for each experiment, a planar surface large enough to be detected by all external sensors simultaneously was used as our object of interest. This allowed us to maximize the accuracy of the pose estimations.

The first experiment had the objective of validating the rules we established for our search algorithm. The experiment consisted of triggering the search algorithm by introducing the object in the field of view of the sensors and allowing the robot to react according to the rules of the algorithm. For this experiment and the last, the object was held in hand by a person attempting to maintain its pose to the best of their ability. To fully test the rules of the algorithm we began by monitoring the behavior of the manipulator robot when no object was present in front of the sensors. According to the rules, no movement should occur. This continues until at least one of the sensors measures a valid distance. Without any valid distance or any prior movement instructions, the robot has no way of predicting in which direction to search for objects and therefore remains stationary. To obtain a uniform search pattern, the manipulator was forced to travel the same total distance in all directions and for this experiment that distance was set to 5 mm.

The second experiment attempted to quantify the error associated with the pose estimation of the external sensor array. In the experiment, the object was positioned in front of the robot's end effector. The object's surface normal was aligned with the world reference frame's Z axis and therefore had no discernable rotational deviations about either of the X or Y axes. A total of 25 pose adjustment iterations were performed. The first 12 iterations consisted of randomly adjusting the distance between the object and the robot by moving the object either toward or away from the end effector. The last 13 iterations consisted of keeping the object stationary. By looking at both of these cases, we were able to examine both the dynamic and static response of the sensor array. For this scenario we made use of our close proximity interaction module. The objective was to match the object's surface orientation in both the X and Y axes and to maintain a constant distance away from the surface of the object.

Our third and final experiment's objective was to examine the robot motion in both the transition and constrained modes by measuring the robot's pose matching capabilities. To evaluate the transition mode, wepositioned a planar surface in a particular pose such that the compliant wrist's external sensors could measure the pose and allow the robot to modify its position in order to match that pose. To evaluate the constrained modewe needed to have the planar surface make contact with the compliant wrist with enough pressure to the contact plate of the wrist to trigger the detection of contact section of the algorithm. By producing a displacement meeting the contact threshold requirements the robot was again able to match the pose of the planar surface.An additional goal was to demonstrate that even in situations where the object being detected is deformable or not completely motionless the robot manipulator is still able to approximatethe desired pose with small deviations.

VI. Results

For the search algorithm experiment, Fig. 9 shows that initially, all of the sensors are returning their maximum distance values. It was mentioned previously that the maximum measurement distance of each sensor is 400 mm but since the external sensors are offset from the contacting surface of the compliant wrist, the offset is subtracted from the total distance measured and results in the 265 mm values shown. The sharp drops in distances correspond to the object coming into the line of sight of each of the sensors. For this case, the valid distance threshold was set to 150 mm. The first sensor to detect an object is sensor 3, followed by sensor 2, then sensor 4 and finally sensor 1. By comparing the order in which each sensor detects the object and the sensor arrangement shown in Fig. 3 we can see that the object first enters the field of view from the +X direction with respect to the end effector. Next, we notice that sensor 2 begins to detect the object while sensor 4 does not. In this case, the search algorithm begins moving in a combined direction of +X and –Y. Once sensor 4 begins to detect an object however, the search direction is again modified until the last sensor in the array, sensor 1, is able to detect the object at which point the motion is halted. When combining the results from Fig. 10, which shows the position corrections made for each of the iterations of the search algorithm, with those of Fig. 9, we are able to see that the

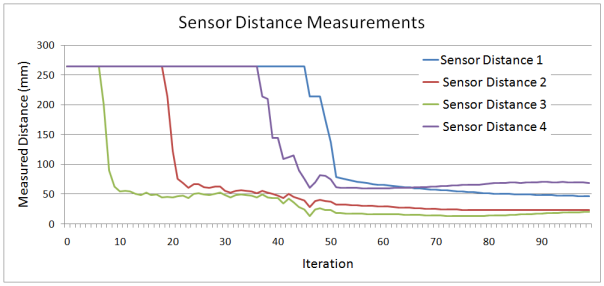

Fig. 9. Sensor distances measured during search algorithm.

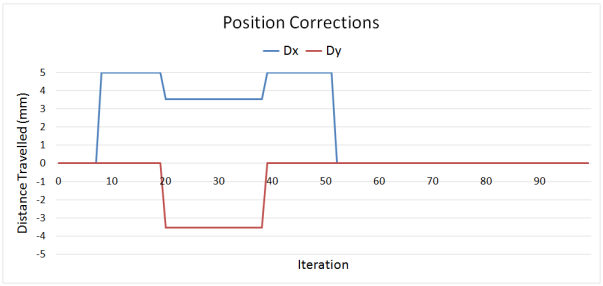

Fig. 10. Position corrections during search algorithm.

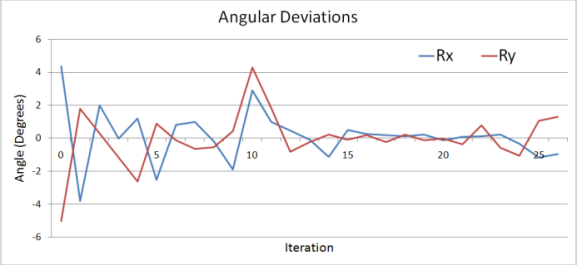

Fig. 11. Angular deviations from desired values.

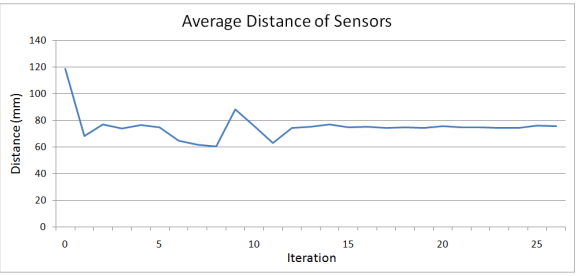

Fig. 12. Average distance of sensors (Target distance = 75 mm).

manipulator does in fact adhere to the rules set forth for the search algorithm.It is important to note that the search algorithm does not attempt to match the pose of the detected object. This combined with the fact thatthe object was being held in place by a person accounts for the largely differing final distance values for each of the sensors.

Fig. 11 and Fig. 12 show the results extracted from the sensors during the operation of the close proximity interaction algorithm. Fig. 11 shows the angular deviation from the desired rotation angle after each iteration of the algorithm and Fig. 12 shows the average distance calculated from the returned values of all four external sensors. The latter is the distance value used in the calculation of the homogeneous transformation matrix upon which the robot relies to control its movements. The desired rotation for both axes was 0 andthe specified distance to maintain was 75 mm. The object was deliberately placed at an initial distance greater than the desired distance we wished to maintain to show that the manipulator could in fact move to the desired position. The resulting mean values obtained for the rotation about the X and Y axes (Rx and Ry) were 0.07 ± 1.85 and 0.30 ± 1.70 degrees for the dynamic iterations, respectively, and -0.15 ± 0.53 and 0.08 ± 0.60 degrees for the static iterations, respectively. The resulting mean value for the average distance to maintain was 71.7 ± 7.7 mm for the dynamic iterations and 75.2 ± 0.7 mm for the static iterations.

Table 2. Pose corrections for motion modes.

Parameter	State	Transition	Transition	Constrained
Tz (mm)	Initial	68.09	33.62	-3.03
	Final	3.08	2.92	-4.30
Rx (°)	Initial	-19.064	5.388	-3.614
	Final	3.488	1.876	-5.600
Ry (°)	Initial	31.897	16.815	-24.649
	Final	-1.437	0.043	4.436

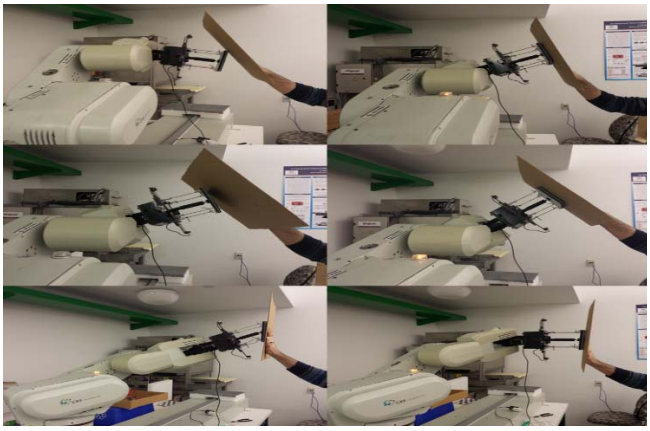

Fig. 13. Robot motion in transition and constrained modes. Top row: transition; middle row: transition; bottom row: constrained.

Results from the third experiment are given in Table 2 which shows a list of the parameters used when generating a transformation matrix to define the desired pose. The data for each of these parameters are extracted directly from the sensor distances of either the internal or external array of sensors, depending on the motion mode, with Tz being the average distance, and Rx, and Ry being the rotation about the X and Y axes, respectively. The state indicates if the values were measure before (initial pose) or after (final pose) updating the manipulator's position. The 3 columns transition, transition and constrained correspond to the first, second and third rows of images in Fig. 13, respectively. In each case, the desired final values of each parameter are all 0 and the values shown are deviations from the desired. The left column of Fig. 13 demonstrates the relative position of the robot and the planar surface before attempting to match the robot's pose to that of the object's surface. The right column shows the relative position once the manipulator has completed its movement into the desired pose.

VII. Discussion

Although much of the literature reviewed in preparation for this work produced interesting and promising results, a direct comparison could not be made due to the novel sensing device used for our experiments. We therefore discuss our findings and address issues which arose throughout the process.

The results of the first experiment are promising due to the low deviations produced for both of the rotations and the translation. Errors such as these can become a concern in certain cases where an extremely high degree of accuracy is required; however, in an unconstrained environment it is quite difficult to eliminate all possible sources of error due to the evolving nature of a human element in a robot's workspace. Moreover, due to the compliance provided by the wrist, the pose estimations need not be as accurate as those required by industrial production processes requiring a high degree of repeatability. One significant source of error in the pose estimation is directly linked to the method of

distance sensing which makes use of reflected infrared light. This method is sensitive to the reflectance of object surfaces as well as ambient lighting. Despite the calibration procedure described in [15] which is meant to improve the accuracy of the individual IR sensors, it is difficult to predict the exact characteristics of each surface that could possibly be encountered in any given situation. The external sensor array is more affected by this type of uncertainty than the internal sensor array. This is due to the fact that the internal sensors need only deal with one type of surface and therefore tend to produce a more stable and accurate output.

As can be seen in Fig. 11, larger errors were detected whenever the target object was continuously changing positions when compared to when the object was kept stationary. This is primarily caused by the delayed response produced by the signal filtering of the sensor inputs. Similar effects were also recorded during the second experiment. Due to the method used for positioning the target during the search algorithm, it is slightly more difficult to discern the primary contributing factor to the sharp changes in the distance measurements. Despite these disturbances, the search algorithm developed was able to successfully locate the intended target.

Our control scheme for close proximity and physical interaction was also successful in estimating the pose of an object and compensating for the difference between the object's pose and the manipulator's pose. The slight errors obtained for both translation and rotation were well within the limits of compliance that the wrist affords the manipulator.

VIII. Conclusion

This work presents a novel real-time system for close proximity and physical human-robot interaction using industrial robots. The main goal of this work was to turn a rigid industrial robot into an adaptable compliant manipulator and to develop a reliable live path planning approach for human-robot collaborative tasks. The proposed method is implementedusing a custom designed instrumented compliant wrist and validated through experimental results with a 7-DOF robotic manipulator. The robot performance was evaluated in three different modes of motion (free motion, transition and constrained) required for human-robot interaction. The results demonstrated that the use of the proposed adaptable compliance control system can improve the safeness of human-robot interactions and that sufficient accuracy is achieved for the robot to detect, follow and interact with a human partner or object. The ability to precisely control the robot pose according to its human partner's behavior using the compliant wrist also allowed an industrial manipulator robot and human to safely and successfully perform physical interaction without major hardware modifications, and no addition of new actuators, internal sensors or costly retrofitting.

References

[1] C. Heyer, "Human-robot interaction and future industrial robotics applications," in *Intelligent Robots and Systems (IROS)*, IEEE/RSJ International Conference on, 2010, pp.4749-4754. doi: 10.1109/IROS.2010.5651294

[2] A. Bicchi, M. Peshkin, and J. Colgate, "Safety for physical human-robot interaction," in *Springer Handbook of Robotics*, B. Siciliano and O. Khatib, Eds. Springer, 2008, pp. 1335-1348.

[3] R.M. Ahmed,"Compliant control of robot manipulator for safe physical human robot interaction," Örebro Universitet, 2011.

[4] M. Quigley, A. Asbeck, and A. Ng, "A Low-Cost Compliant 7-DOF Robotic Manipulator," in *Proc. of IEEE Intl Conf. on Robotics andAutomation*, 2011, pp. 6051-6058.

[5] M. Laffranchi, N. Tsagarakis, and D. Caldwell,"CompAct Arm: a Compliant Manipulator with Intrinsic Variable Physical Damping," In *Robotics: Science and Systems*,vol. 8, pp. 225-232, 2013.

[6] M.A. Goodrich and A.C. Schultz, "Human-Robot Interaction: A Survey." *Foundations and Trends in Human-Computer Interaction,* vol. 1. No. 3,pp. 203-275, February 2007.

[7] K.J.M. Yeoh and H. L. Wong, "Web-based remote navigational robot for multiclass human-robot interaction," In *IEEE Conference on Sustainable Utilization and Development in Engineering and Technology (STUDENT)*, 2012, pp. 170-175.

[8] D. Nakhaeinia, R. Fareh, P. Payeur, and R. Laganière, "Trajectory planning for surface following with a manipulator under RGB-D visual guidance," In *IEEE International Symposium on Safety, Security, and Rescue Robotics (SSRR)*,2013, pp.1-6,. doi: 10.1109/SSRR.2013.6719365.

[9] Q. Kun, J. Niu, and H. Yang, "Developing a Gesture Based Remote Human-Robot Interaction System Using Kinect", *International Journal of Smart Home*, vol. 7, no. 4, July 2013.

[10] P. A. Lasota, G. F. Rossano, andJ. A. Shah "Toward Safe Close-Proximity Human-Robot Interaction with Standard Industrial Robots," in *the 10th IEEE International Conference on Automation Science and Engineering* (CASE), Taipei, Taiwan,2014.

[11] P. A. Lasota and J. A.Shah, "Analyzing the Effects of Human-Aware Motion Planning on Close-Proximity Human–Robot Collaboration," Massachusetts Institute of Technology, Cambridge, Massachusetts, HUMAN FACTORS. pp. 1–13. DOI: 10.1177/0018720814565188.

[12] J. Mainprice and D. Berenson, "Human-robot collaborative manipulation planning using early prediction of human motion,"in *IEEE/RSJ International Conference on Intelligent Robots and Systems*, 2013, pp. 299-306.

[13] S. Ikemoto, T. Minato, and H. Ishiguro, "Analysis of physical human-robot interaction for motor learning with physical help," *Appl. Bionics Biomech. (Special Issue on Humanoid Robots)*, vol. 5, no. 4, pp. 213-223, 2008.

[14] S. Ikemoto, H.B. Amor, T. Minato, B. Jung, and H. Ishiguro, "Physical Human-Robot Interaction: Mutual Learning and Adaptation," *Robotics & Automation Magazine, IEEE*, vol.19, no.4, pp.24-35, Dec. 2012. doi: 10.1109/MRA.2011.2181676.

[15] S.Norouzzadeh, T. Lorenz and S. Hirche, "Towards safe physical human-robot interaction: An online optimal control scheme," *RO-MAN, IEEE*, 2012, pp.503-508.

[16] P. Laferrière, P. Payeur, and R. Toledo, "Instrumented Compliant Wrist for Dexterous Robotic Interaction," in *IEEE Intl Symposium on Robotic and Sensors Environments (ROSE)*,2014, pp. 66-71.

[17] R. Fareh, P. Payeur, D. Nakhaeinia, R. Macknojia, A. Chavez-Aragon, A.-M.Cretu, P. Laferrière, R. Laganière and R. Toledo,"An integrated vision-guided robotic system for rapid vehicle inspection," in *8th Annual IEEE Systems Conference (SysCon)*,2014, pp.446-451. doi: 10.1109/SysCon.2014.6819295.